AGU PUBLICATIONS

JGR

Journal of Geophysical Research: Atmospheres

RESEARCH ARTICLE

10.1002/2014JD021667

Key Points:

- Land albedo climatologies were derived from nine global satellite data sets
- Most satellite albedos can be used for model calibration and validation
- Large differences were found at high latitudes between satellite data sets

Supporting Information:

- Readme
- Figure S1

Correspondence to:
T. He,
the@umd.edu

Citation:
He, T., S. Liang, and D.-X. Song (2014), Analysis of global land surface albedo climatology and spatial-temporal variation during 1981–2010 from multiple satellite products, *J. Geophys. Res. Atmos.*, *119*, 10,281–10,298, doi:10.1002/2014JD021667.

Received 19 FEB 2014
Accepted 16 AUG 2014
Accepted article online 20 AUG 2014
Published online 11 SEP 2014

Analysis of global land surface albedo climatology and spatial-temporal variation during 1981–2010 from multiple satellite products

Tao He[1], Shunlin Liang[1,2], and Dan-Xia Song[1]

[1]Department of Geographical Sciences, University of Maryland, College Park, Maryland, USA, [2]State Key Laboratory of Remote Sensing Science, College of Global Change and Earth System Science, Beijing Normal University, Beijing, China

Abstract For several decades, long-term time series data sets of multiple global land surface albedo products have been generated from satellite observations. These data sets have been used as one of the key variables in climate change studies. This study aims to assess the surface albedo climatology and to analyze long-term albedo changes, from nine satellite-based data sets for the period 1981–2010, on a global basis. Results show that climatological surface albedo data sets derived from satellite observations can be used to validate, calibrate, and further improve surface albedo simulations and parameterizations in current climate models. However, the albedo products derived from the International Satellite Cloud Climatology Project and the Global Energy and Water Exchanges Project have large seasonal biases. At latitudes higher than 50°, the maximal difference in winter zonal albedo ranges from 0.1 to 0.4 among the nine satellite data sets. Satellite-based albedo data sets agree relatively well during the summer at high latitudes, with a standard deviation of 0.04 for the 70°–80° zone in both hemispheres. The fine-resolution (0.05°) data sets agree well with each other for all the land cover types in middle to low latitudes; however, large spread was identified for their albedos at middle to high latitudes over land covers with mixed snow and sparse vegetation. By analyzing the time series of satellite-based albedo products over the past three decades, albedo of the Northern Hemisphere was found to be decreasing in July, likely due to the shrinking snow cover. Meanwhile, albedo in January was found to be increasing, likely because of the expansion of snow cover in northern winter. However, to improve the albedo estimation at high latitudes, and ultimately the climate models used for long-term climate change studies, a still better understanding of differences between satellite-based albedo data sets is required.

1. Introduction

Surface albedo, a variable defined as the ratio of the solar radiation reflected from Earth's surface to the solar radiation incident upon it, is critical to the regulation of Earth's surface energy budget [*Liang et al.*, 2010, 2013a]. Land surface albedo is highly variable, both spatially and temporally. Significant changes in surface albedo are accompanied by variations in land cover and surface conditions, such as snow [*He et al.*, 2013], vegetation [*Loarie et al.*, 2011; *Lyons et al.*, 2008], urbanization [*Offerle et al.*, 2005], and soil moisture [*Govaerts and Lattanzio*, 2008; *Zhu et al.*, 2011]. B. Ghimire, et al. (Global albedo change and radiative cooling from anthropogenic land-cover change, 1700 to 2005 based on MODIS, land-use harmonization, radiative kernels, and reanalysis, submitted to *Geophysical Research Letters*, 2014). estimated global surface albedo change, taking into account land cover change. They found that the global surface albedo increased 0.0012 during 1700–2005, which had a net cooling effect of a top-of-atmosphere (TOA) radiative forcing of $-0.23\ \mathrm{W\,m^{-2}}$. Aerosols like dust and soot may also contaminate snow and greatly reduce its albedo [*Hansen and Nazarenko*, 2004; *Xu et al.*, 2009]. Accurate surface albedo data are needed to better characterize climate systems and to help develop climate models with improved predictive power.

Satellite data provide a unique opportunity for monitoring surface albedo on a global basis [*Liang et al.*, 2012]. Algorithms for albedo estimation have been developed for various different types of remote sensing sensors and platforms, from broadband sensors [e.g., *Li and Garand*, 1994; *Pinty et al.*, 2000] to multispectral [e.g., *Csiszar and Gutman*, 1999; *He et al.*, 2012; *Schaaf et al.*, 2002; *Shuai et al.*, 2014; *Wang et al.*, 2013], multiangle [e.g., *Maignan et al.*, 2004; *Martonchik et al.*, 1998], and hyperspectral [*He et al.*, 2014a] sensors. During the past few decades, many long-term albedo products with global coverage have been derived from satellite data (Tables 1 and 2).

Table 1. Global Satellite Albedo Products Used in This Study

Albedo Data Sets	Input Source	Resolution	Frequency	Temporal Coverage	Type of Albedo
GLASS	AVHRR and MODIS	0.05°	8 day	1981 to present	BSA and WSA
GlobAlbedo	AATSR, MERIS, VGT, and MODIS	0.05°	Monthly	1998–2011	BSA and WSA
MERIS	MERIS	0.25°	Monthly	2002–2006	BSA
MODIS	MODIS	0.05°	8 day	2000 to present	BSA and WSA
CLARA-SAL	AVHRR	0.25°	10 day and Monthly	1982–2009	BSA
ERBE	ERBE	2.5°	Monthly	1985–1989	BSA

Surface albedo products with an absolute accuracy of 0.02–0.03 are generally required for regional and global climate studies [*Dozier et al*., 1989; *Sellers et al*., 1995]. As climate modeling techniques have advanced in recent decades by introducing temporally involved albedo parameterizations, albedo accuracy requirements have generally changed to be more specific based on the time and location of the applications [e.g., *Loew et al*., 2014; *Wang et al*., 2007; *Widlowski et al*., 2011]. Comparisons of satellite-based albedo data sets with general circulation models (GCMs) have been made in previous studies [*Oleson et al*., 2003; *Wang et al*., 2006; *Wang et al*., 2004; *Wang and Zeng*, 2010; *Zhang et al*., 2010; *Zhou et al*., 2003]. For example, *Wang et al*. [2006] compared results from the Coupled Model Intercomparison Project Phase 3 (CMIP3) models with data from the International Satellite Cloud Climatology Project (ISCCP) for the period 1984–1999 and found that the modeled albedo was systematically overestimated by as much as 0.05 in summer, compared to the ISCCP data. *Zhang et al*. [2010] compared the Moderate Resolution Imaging Spectroradiometer (MODIS) albedo products with the results from CMIP3 models for the period 2000–2008 and found that differences in annually averaged global albedo can be as large as 0.06. However, a thorough comparison between global long-term satellite-based albedo data sets has not yet been attempted.

Surface albedo varies both spatially and temporally. *Fang et al*. [2007] calculated the variation of albedo over the continent of North America for different plant function types (PFTs) using MODIS time series and generated the shortwave albedo climatology for each of the PFTs. They observed that the within-class standard deviation (SD) shows a strong seasonal character; that is, the SD increases in winter and spring and decreases in the growing season. They also found the strong link between maximal variation in surface albedo and events such as winter snowfall and spring snowmelt. *Zhang et al*. [2010] analyzed a MODIS albedo time series to map global albedo variation and found a decrease of ~0.01 in land surface albedo for the Northern Hemisphere for the period 2000–2008. *Gao et al*. [2005] found that the interannual variation of the MODIS shortwave albedo is less than 0.01 over snow-free surfaces suggesting that the albedo trend is possibly associated with land surface changes in cryosphere.

Surface albedo may change with land cover dynamics caused by deforestation, afforestation, urbanization, snowfall, snowmelt, etc. Previous studies have demonstrated changes in surface albedo at various different locations throughout the past three decades [e.g., *He et al*., 2013; *Shi and Liang*, 2013]. The Northern Hemisphere, which contains most of Earth's land surface and about 90% of the total population, is believed to have been affected by recent climate changes. Surface albedo changed dramatically for the Northern Hemisphere with different trends in winter and summer during the past decades. Many studies have reported warming trends due to climate change in the Northern Hemisphere in recent decades [e.g., *Flanner et al*., 2011; *He et al*., 2013; *Jeong et al*., 2011]. It is therefore useful to offer a brief trend analysis to help identify the magnitude and contributors of surface albedo changes from multiple data sets used in this study and to further improve climate models to better capture the surface changes.

The main objective of this study is to identify the differences and potential issues of the existing global satellite albedo data sets and make possible suggestions to modeling communities when facing data set selection for model validation and calibration purposes. Because most previous studies focused on a relatively short

Table 2. Global Satellite Surface Shortwave Radiation Products Used in the Comparison

Albedo Data Sets	Full Name	Spatial Resolution	Temporal Coverage
GEWEX	Global energy and water exchanges project	1°	1983–2007
ISCCP	International satellite cloud climatology project	280 km (2.5°)	1983–2009
CERES	Clouds and Earth's radiant energy system	1°	2000–2012

period in analyzing the climatological surface albedo, we did so for a period of 30 years (1981–2010) in this study. We compared nine long-term global satellite-based albedo data sets, discussed the issues of each data set, and performed a brief trend analysis of land surface albedo. Section 2 introduces each albedo data set used for in the comparison as well as the methodology for albedo calculation and comparison, which is followed by the climatological and trend analysis and discussions in section 3.

2. Data and Method

2.1. Global Long-Term Satellite Albedo Products

2.1.1. MODIS

The MODIS sensors on Terra and Aqua provide measurements on a global basis every 1 or 2 days with seven spectral bands in the shortwave range for land applications. Currently, MODIS albedo products are generated every 8 days since early 2000 [*Gao et al*., 2005; *Schaaf et al*., 2002]. The atmospherically corrected surface reflectance data during a 16 day compositing period are collected as the input of the kernel models to calculate surface albedo. Albedo and the corresponding quality data are available at 500 m resolution in sinusoidal projection and 0.05° in latitude/longitude projection. Both black-sky albedo (BSA) and white-sky albedo (WSA) are provided through the MCD43 data set. The Collection 5 MCD43C product was used in this study.

MODIS albedo products have been validated extensively [*Cescatti et al*., 2012; *He et al*., 2012; *Liu et al*., 2009; *Roman et al*., 2013; *Stroeve et al*., 2005; *Z Wang et al*., 2012]. They have been widely used as a benchmark for evaluating other satellite albedo products.

2.1.2. MERIS

A global albedo climatology was generated using the Medium-Resolution Imaging Spectrometer (MERIS) data for the period 2002–2006 [*Popp et al*., 2011], which was designed for the estimation of cloud fraction for the Fast Retrieval Scheme for Clouds from the Oxygen A-band (FRESCO+) algorithm. MERIS BSA data from the period October 2002 to October 2006 were aggregated to a grid of 0.25° × 0.25° for each month of the year and for different spectral channels [*Popp et al*., 2011]. In this study, the conversion from spectral to shortwave broadband albedo used for MERIS was based on the empirical equation derived by *Liang* [2001].

2.1.3. GLASS

The Global Land Surface Satellites (GLASS) albedo product from 1981 is produced from advanced very high resolution radiometer (AVHRR) and MODIS data [*Liang et al*., 2013b]. The GLASS albedo product from MODIS observations is based on two direct albedo estimation algorithms, one designed for surface reflectance and one for TOA reflectance [*Qu et al*., 2014], and the statistics-based temporal filtering fusion algorithm is used to integrate these two albedo products [*Liu et al*., 2013a]. The GLASS albedo product from AVHRR observations is based on a direct estimation algorithm using the surface reflectance with radiometric calibration and atmospheric correction [*Pedelty et al*., 2007] comparable to that used on MODIS data [*Liu et al*., 2013b]. Global albedo maps derived from AVHRR and MODIS are available at a resolution of 0.05° (~5 km) every 8 days. In addition, albedo data at 1 km resolution in sinusoidal projection derived from MODIS observations are provided at the same temporal resolution. Both BSA and WSA are provided in the GLASS albedo product.

The GLASS albedo product has been evaluated using ground measurements and the MODIS albedo product in previous studies [*He et al*., 2013; *Liu et al*., 2013b]. The evaluations show that GLASS albedo has an accuracy that is comparable to that of MODIS albedo product and that this has been the case consistently throughout the period of 1981–2012.

2.1.4. GlobAlbedo

The GlobAlbedo project aims to provide global surface albedo data for the period of 1998–2011 based on European satellites at three different spatial resolutions from 1 km, 0.05° to 0.5°. Data derived from the Advanced Along-Track Scanning Radiometer (AATSR), SPOT4-VEGETATION, SPOT5-VEGETATION2, and MERIS are integrated using an optimal estimation approach [*Lewis et al*., 2013] and a gap-filling technique based on the MODIS surface anisotropy data set [*Lewis et al*., 2013; *Muller et al*., 2012]. Both BSA and WSA are provided in GlobAlbedo product. In this study, the monthly GlobAlbedo data at a 0.05° resolution were used. Preliminary validation of GlobAlbedo products showed a generally good agreement against MODIS albedo products with an R^2 of 0.85 on a global basis; however, problems with snow detection at high latitudes (>70°) were found to cause significant artifacts in the final product [*Muller*, 2013].

2.1.5. CLARA-SAL

The time series from the Clouds, Albedo, and Radiation-Surface Albedo (CLARA-SAL) provide the global shortwave BSA for the period 1982–2009, derived from AVHRR sensors [*Riihela et al*., 2013]. The CLARA-A1-SAL (AVHRR First Release) was used in this study. Atmospheric effects were corrected using the simplified method for atmospheric correction [*Rahman and Dedieu*, 1994], assuming a constant value of 0.1 for the aerosol optical depth (AOD) and an ozone constant of 0.35 cm. For vegetated surfaces, shortwave broadband albedo was converted from spectral albedo [*Liang*, 2001] after removing the surface anisotropic effects [*Wu et al*., 1995]. For snow and ice surfaces, broadband albedo was directly converted from surface reflectance at a spatial resolution of 0.05° following the method of *Xiong et al*. [2002] and then averaged to calculate the monthly means at a spatial resolution of 0.25°. Efforts were made to provide a temporally consistent data set from different AVHRR sensors, by considering corrections for sensor calibration and orbital drift [*Heidinger et al*., 2010]. This product has been validated thoroughly against ground measurements at spatially representative sites around the world showing a relative uncertainty of 11% in the monthly albedo estimation [*Riihela et al*., 2013]. They also found that using a constant AOD value of 0.1 at 550 nm led to a typical overestimation of 5–10% in surface albedo [*Riihela et al*., 2013].

2.1.6. ERBE

Surface albedo has been generated from the broadband Earth Radiation Budget Experiment (ERBE) sensors on board two polar-orbiting NOAA satellites and one Earth Radiation Budget Satellite (ERBS) [*Li and Garand*, 1994]. Estimated from the satellite observations by the scene-dependent angular models, the ERBE TOA albedo was used to derive surface albedo with the empirical relationship established based on radiative transfer simulations with a constant AOD of 0.05 at 550 nm. Validation of the instantaneous surface albedo from the ERBE observations at two agricultural sites showed a bias of 0.01 with a root-mean-square error (RMSE) of 0.03 [*Li and Garand*, 1994]. *Jin et al*. [2003] reported a 0.90 correlation with an RMSE of 0.047 between MODIS and ERBE albedos. Monthly climatology of the ERBE surface albedo used in this study was calculated from the clear-sky observations obtained during 1985–1989 and available at a spatial resolution of 2.5° covering the regions from 60°N to 60°S [*Li and Garand*, 1994].

2.2. Albedo From Global Long-Term Surface Shortwave Radiation Data Sets

2.2.1. ISCCP

The International Satellite Cloud Climatology Project's (ISCCP) flux data set-monthly mean of profiles of radiative fluxes data set provides monthly global surface shortwave radiation budget estimates at a spatial resolution of 2.5° (~280 km) from July 1983 to December 2009 [*Zhang et al*., 1995; *Zhang et al*., 2004]. Comparisons of surface albedo from ISCCP against other radiation data sets indicate that ISCCP data have a general underestimation of land surface albedo on a global basis, particularly in tropical regions [*Stackhouse et al*., 2012].

2.2.2. GEWEX

The Global Energy and Water Exchanges Project's (GEWEX) surface radiation budget (SRB) product version 3.0 was produced by the National Aeronautics and Space Administration (NASA)/GEWEX to facilitate study of Earth's radiation budget under global and regional climate change. The SRB data set has a temporal coverage of 24.5 years, from July 1983 to December 2007, at a spatial resolution of 1°. The shortwave radiation data are estimated using the algorithms developed by *Pinker and Laszlo* [1992], which requires cloud property inputs from ISCCP, reanalysis temperature and moisture from the fourth Goddard Earth Observing System Model (GEOS-4), and ozone observations from multiple satellites. Validations of GEWEX surface albedo with other radiation data sets showed an underestimation of GEWEX albedo over snow/ice surfaces [*Qin et al*., 2011; *Stackhouse et al*., 2012].

2.2.3. CERES

The latest monthly shortwave radiation data from the Clouds and the Earth's Radiant Energy System (CERES) sensors on board Terra and Aqua are available at a spatial resolution of 1°, from March 2000 to September 2012, using MODIS surface anisotropy data as background information. CERES products include both clear-sky and all-sky shortwave radiation estimates. We chose the most recent CERES Edition 2.7r all-sky surface downward and upward radiation from the Energy Balanced and Filled (EBAF) data set [*Kato et al*., 2013] to calculate the blue-sky albedo in this study. Broadband albedos derived from CERES data have been validated in previous studies, which revealed an underestimation of 0.003–0.008 relative to MODIS albedos [*Hudson et al*., 2010; *Rutan et al*., 2009]. *Kato et al*. [2013] evaluated the uncertainties in the CERES-derived irradiance with satellite-derived cloud and aerosol properties and found that the monthly mean upward shortwave radiation over land could have uncertainties of 12 W m^{-2} at a grid level, which can be translated into an error of 0.06 in surface albedo given the mean downward shortwave radiation of 203 ± 12 W m^{-2}.

2.3. Calculation of Global and Regional Average Albedo

Earth's surface albedo (blue-sky albedo) is the ratio of the reflected solar radiation to the incident solar radiation. Thus, it is temporally and spatially scalable. To calculate the blue-sky surface albedo over a region, monthly averaged data are spatially aggregated following equation (1), for which we need to consider the downward radiation. For those data sets that only provided BSA, equation (2) was used to calculate the spatial mean albedo.

$$\overline{\alpha} = \frac{\sum A^i F_d^i \left[\left(1 - f_{\mathrm{dif}}^i\right) \alpha_{\mathrm{bs}}^i + f_{\mathrm{dif}}^i \alpha_{\mathrm{ws}}^i \right]}{\sum A^i F_d^i}, \tag{1}$$

$$\overline{\alpha} = \frac{\sum A^i F_d^i \alpha_{\mathrm{bs}}^i}{\sum A^i F_d^i}, \tag{2}$$

where $\overline{\alpha}$ is the spatially aggregated shortwave albedo. For pixel i, A^i is the area of the pixel, F_d^i is the surface downward radiation under all-sky condition, f_{dif}^i is the diffuse skylight ratio, and α_{bs}^i and α_{ws}^i are the BSA and WSA, respectively.

Although downward radiation data from GEWEX have been used for the purpose of spatial aggregation of albedo before [*Zhang et al*., 2010], estimation of downward radiation over bright surfaces [*Gui et al*., 2010] may result in inaccurate albedo estimates at high latitudes. Instead, we used the monthly downward radiation data from the Modern-Era Retrospective Analysis for Research and Applications (MERRA) reanalysis to calculate the spatial mean albedo in equations (1) and (2) at a finer spatial resolution of 1/2° × 2/3° [*Rienecker et al*., 2011].

Differences between BSA and blue-sky albedo have been shown to be very small over snow-free surfaces when the solar zenith angle is less than 70° [*Liu et al*., 2009]. However, the importance of the coupling of diffuse downward radiation in surface albedo estimation has been emphasized [*Pinty et al*., 2005; *Roman et al*., 2010], particularly for snow-covered surfaces. In previous studies, the diffuse skylight ratio has been either ignored or assumed constant in the calculation of the blue-sky albedo [*Zhang et al*., 2010]. To improve the albedo estimation over large regions, we used monthly diffuse and direct downward radiation data from the National Centers for Environmental Prediction (NCEP) reanalysis [*Kalnay et al*., 1996] to derive the diffuse skylight ratio in equation (1). Figure 1 shows the diffuse skylight ratio in the total shortwave range, derived from NCEP data. It indicates that the diffuse skylight ratio is not constant but that it varies over both time and space. We have aggregated albedos using both MERRA and NCEP downward radiation data as inputs in equation (1). Despite the difference in the spatial resolution, the correlation between albedos aggregated up to the global level based on these two data sets was found to be 0.994 at the 99% confidence level.

To consistently prevent ocean pixels from corrupting the land surface albedo calculation over the time period in this study, we used the MODIS land cover map (MCD12C1) of 2000 to identify and exclude the same ocean pixels for each temporal observation. The land and ocean information from the original MODIS land cover data at a 0.05° resolution was directly applied on the GLASS, MODIS, and GlobAlbedo data to screen the nonland pixels. We aggregated the land cover data to match the spatial resolutions for all the other data sets based on a majority rule: if the majority of the fine-resolution pixels to be aggregated are land, the corresponding coarse-resolution pixels were masked as land. Because CLARA-SAL albedo was first generated at a spatial resolution of 0.05° including sea ice pixels and then aggregated to 0.25° in its publicly released product [*Riihela et al*., 2013], it is highly likely that the CLARA-SAL albedo aggregated in this study will cause an overestimation compared with other fine-resolution land albedo products if we applied the majority rule in spatial aggregation.

Unlike the other data sets that are available on a monthly basis, GLASS and MODIS products are provided at 8 day intervals. To get comparable monthly mean albedo from these two data sets and to maintain high-quality albedo data, only the albedo data with quality flags of 0 and 1 were included in the calculation for these two data sets.

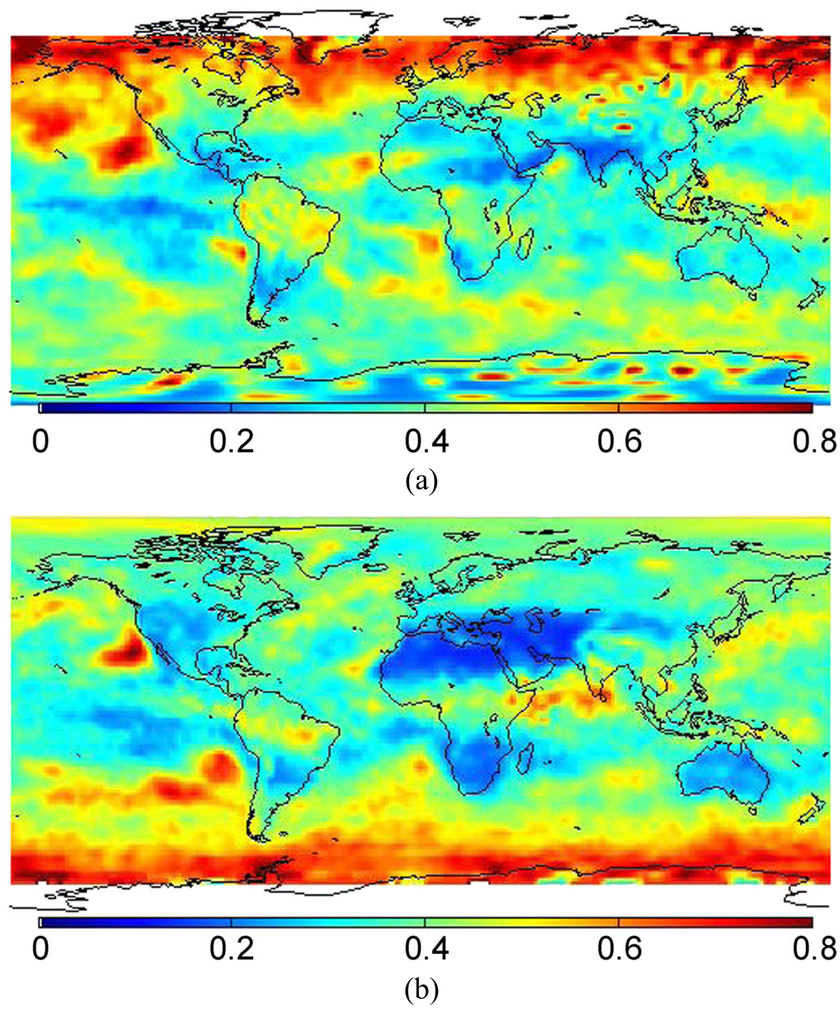

Figure 1. Global diffuse skylight ratio derived from NCEP data for (a) January 2000 and (b) July 2000.

3. Results and Discussion

3.1. Land Surface Albedo Climatology

3.1.1. Global Land Surface Albedo

Monthly albedo averages were calculated for each of the data sets mentioned in section 2 except for the ERBE data due to its spatial coverage. As can be seen from the global values shown in Figure 2a, most of the satellite albedo products agree relatively well and can likely satisfy the accuracy requirements for global climate applications, with differences less than 0.02. *Fang et al*. [2007] found that in North America albedo increases in winter and spring and decreases in the growing season. It is interesting to find that the mean surface albedo for the Northern Hemisphere peaks in March (Figure 2b). This can be explained by the fact that high-latitude regions on the Northern Hemisphere receive little amount of downward solar radiation ($<5\ \mathrm{W\,m^{-2}}$) in winter. Consequently, strongly reflective surfaces common to these latitudes, such as snow and ice, do not actively contribute to the shortwave radiation budget. From winter to spring, increasingly high surface albedos are observed, because snow and ice contribute to the radiation budget more and more as a result of increasing exposure to sunlight. Based on the result of our climatology comparison, we can conclude that most of the satellite-based albedo data sets shown in Figure 2 can serve as the background information in global long-term climate modeling studies.

Although mismatch exists within temporal coverages among the selected data sets, the magnitude of difference among the derived albedo climatologies is significantly larger than that of the three decadal changes in global mean land surface albedo (see section 3.2). Thus, it is reasonable to compare the climatologies derived

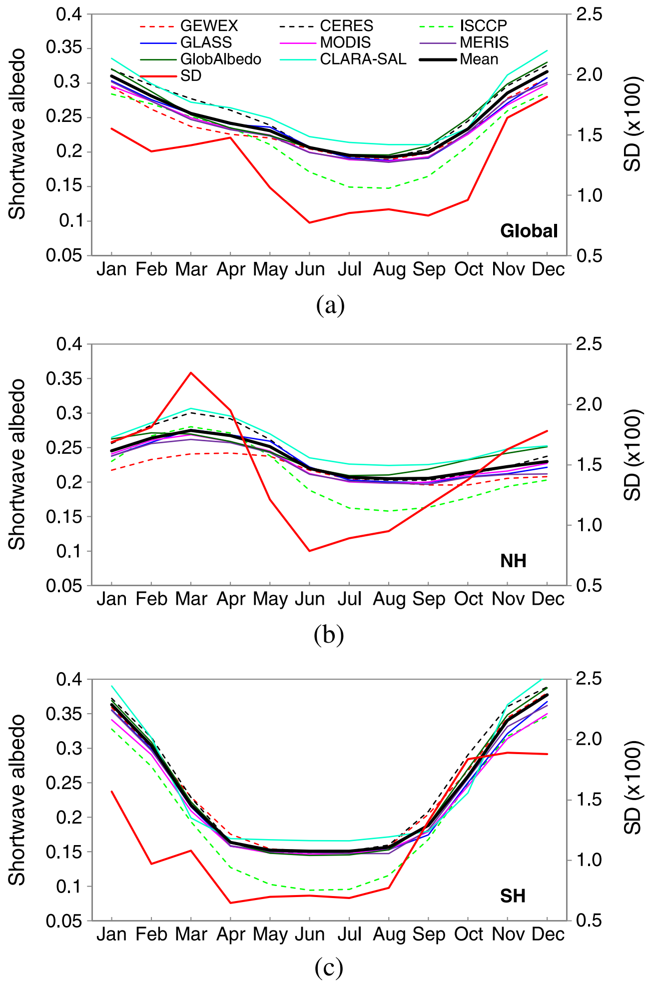

Figure 2. Monthly climatological surface shortwave albedo derived from satellite-based albedo data sets for (a) the globe, (b) the Northern Hemisphere, and (c) the Southern Hemisphere. The "mean" and "SD" are calculated from all the data sets except the ISCCP.

from these data sets with different temporal coverages. ISCCP climatological albedos were found to be considerably underestimated, particularly from June to September. This confirms the finding of *Wang et al.* [2006] that the GCM simulation results overestimated surface albedos, relative to ISCCP albedos by about 0.05 in summer at northern latitudes. Based on results from other satellite products shown in this study (Figure 2), it is likely that ISCCP surface albedos were negatively biased, particularly from June to August for both hemispheres. An intercomparison made among the CERES, GEWEX, and ISCCP surface shortwave radiation data suggested that the underestimation of ISCCP surface albedo in middle to low latitudes was possibly the result of inaccurate estimation on atmospheric transmittance over urban and tropical regions [*Stackhouse et al.*, 2012]. *Stackhouse et al.* [2012] also pointed out that GEWEX had significant underestimation in albedo over snow/ice surfaces, which is likely the reason of its underestimation in winter and early spring shown in Figure 2.

The CLARA-SAL albedo product tends to have the highest values in most seasons for both hemispheres. There are three reasons for this overestimation. First, the CLARA-SAL product includes sea ice albedo estimates, which may affect our regional aggregates. Its coarse resolution is likely to result in mixed pixels from sea ice and land cover. It matched the data from CERES very well, which is a coarse-resolution data set with pixels mixed from sea ice and land covers and believed to be more accurate than ISCCP and GEWEX [*Stackhouse et al.*, 2012]. Second, the CLARA-SAL product provides only the BSA, which is typically with higher value than the actual "blue-sky" albedo, if the solar zenith angle is large. Third, the weaker cloud detection ability of the AVHRR sensors makes it more likely for cloud pixels to be misidentified as snow/ice pixels at latitudes higher than 50° [*Karlsson et al.*, 2013], leading to overestimation of surface albedo.

Differences between the albedo data sets range from approximately 3% to 5% (not considering the ISCCP data) depending on the season and location. In the Northern Hemisphere, surface albedo peaks in March and April, when the amount of snow cover exposed to sunlight reaches its maximum. Not surprisingly, differences in albedo also peak for the same season with SD $>$ 0.02 (Figure 2b). For the Southern Hemisphere, these data sets were not in good agreement from October to January with SD $>$ 0.015 (not considering the ISCCP data), which likely resulted from the large differences in albedo over the Antarctic region (Figure 3).

Differences between the albedo data sets were found to be larger for the Northern Hemisphere (Figure 2b) than for the Southern Hemisphere (Figure 2c). This is likely because seasonal snow cover is more extensive in the Northern than in the Southern Hemisphere. Thus, for the Southern Hemisphere, estimation accuracy of the aggregated albedos would suffer less from uncertainties in the snow cover detection and parameterization of snow albedo. Disagreement on spring albedo for the northern high latitudes could be

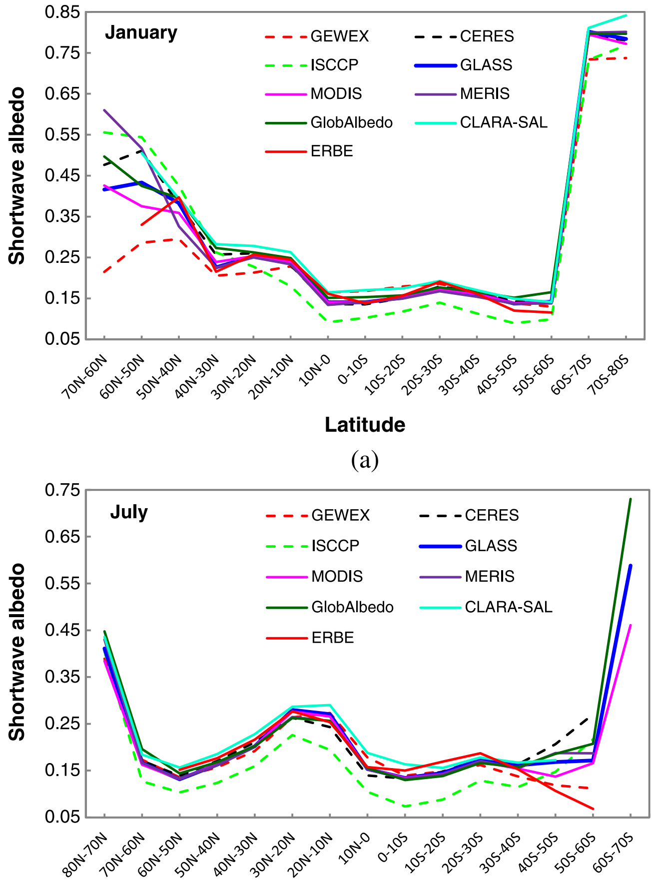

(a)

(b)

Figure 3. Climatological surface shortwave albedo at different latitudes for (a) January and (b) July.

attributed to a high degree of sensitivity of the land surface albedo to the different spatial resolutions (e.g., partial/subpixel snowmelt) and temporal composition strategies used in the different albedo data sets [*He et al.*, 2013]. In addition, changes in plant phenology, poleward expansion of tree line, and other climate-related variations are more prominent and complex in the Northern Hemisphere increasing the uncertainties in the climatological comparison of surface albedo data sets [*Davidson and Wang*, 2005; *MacDonald et al.*, 2008; *Maignan et al.*, 2008; *Wang and Davidson*, 2007].

Differences in absolute sensor calibration and narrowband-to-broadband conversion may also lead to biases in climatological surface albedo values derived from these data sets [*Govaerts et al.*, 2006; *Loew and Govaerts*, 2010]. However, complex error propagation in the radiative transfer and surface anisotropy modeling makes it difficult to directly analyze their effects on surface albedo estimation, which needs further efforts.

3.1.2. Zonal Surface Albedo

The zonal mean albedo was also calculated to help further identify differences between the various albedo data sets. Figure 3 shows the zonal mean albedo of 70°N–80°S in January and 80°N–70°S in July using 10° intervals. Most albedo data sets agree well with each other in middle to low latitudes, except for ISCCP albedos. In addition to finding that ISCCP albedos were considerably underestimated as discussed in section 3.1.1, we also found that GEWEX surface albedos were considerably underestimated in winter at latitudes higher than 50°. Only a few satellite-based albedo data sets have valid values for observations made in winter at latitudes higher than 60° in the Southern Hemisphere. For the latitudinal zones from 40°S to 60°S, the small land surface area may lead to the difference in albedo data sets in Figure 3, which is possibly a result of the differences in spatial resolutions.

For both hemispheres, satellite-based albedo data sets were found to be substantially inconsistent in winter at high latitudes. At latitudes higher than 50°, the maximal difference in winter zonal albedo ranges from 0.1 to 0.4 between satellite-based data sets. Differences in the handling of observations with large solar zenith angle in surface anisotropy modeling may lead to significant differences in albedo estimation for these data sets, because errors in albedo estimations tend to increase with solar zenith [*Liu et al.*, 2009]. On the other hand, albedo estimates made in summer agree very well for both hemispheres at high latitudes. For example, the SD is approximately 0.04 for the 70°–80° zone, which can be converted to the relative value of 5.27% for January in the Southern Hemisphere and 9.88% for July in the Northern Hemisphere. The differences among the satellite-based albedo data sets at high latitudes were likely caused by difficulties in correctly distinguishing between clouds and snow using optical remote sensing imagery (leading to misclassification of pixels), by differences in snow albedo retrieval algorithms (e.g., the MODIS albedo algorithm tends to generate a snow-free albedo if the majority of observations in the temporal composite is

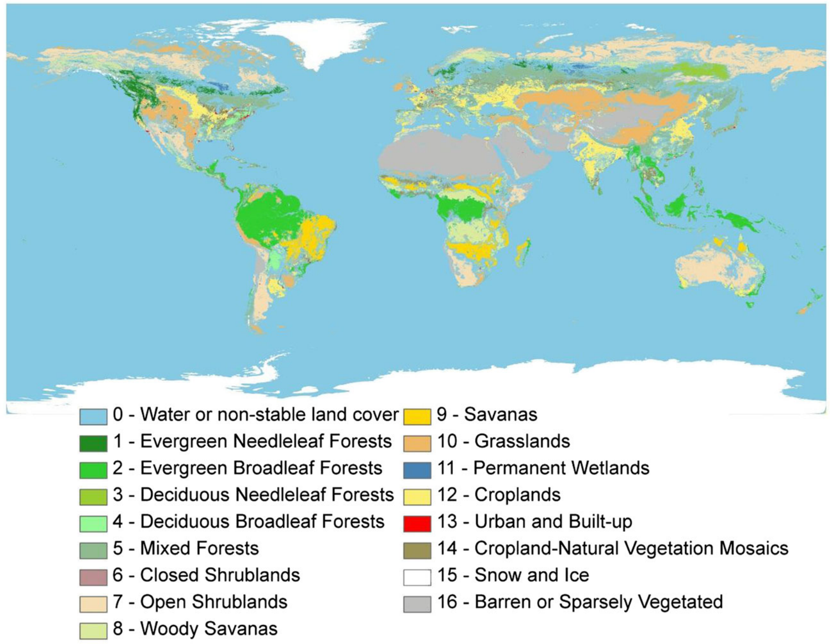

Figure 4. Multiyear stable land cover map derived from MODIS product 2001–2010. Pixels with nonzero values had the same land cover type from MODIS land cover product during the period of 2001–2010.

free of snow), and by differences in spatial resolutions. The cutoff angle and angle normalization in satellite products may also contribute to the large difference in albedo for high-latitude regions.

Among all the nine data sets, GLASS albedo has the best agreement with MODIS albedo. A slightly larger difference among them was found in snow cover transition region 40°N–60°N in January, which is probably a result of their differences in snow albedo retrieval algorithms. The MODIS albedo algorithm tends to generate a snow-free albedo if the majority of observations in the temporal composite is free of snow, whereas the GLASS albedo product uses a temporal filter to smooth the daily albedo and then calculate the 16 day mean albedo, which is more likely to have included the albedo from ephemeral snow resulting in a higher albedo than the MODIS product [*Liu et al.*, 2013b].

MERIS albedo climatology also showed consistent values with MODIS and GLASS products in terms of zonal averages, except for the high northern latitudes (>50°N) in January. This is because the MERIS algorithm relies on the MODIS aerosol product for atmospheric correction and uses MODIS surface anisotropy information in its retrieval procedure. The overestimation of MERIS albedo in high-latitude winter has also been found in *Fischer et al.* [2009], which was, however, attributed to the inaccurate atmospheric correction.

GlobAlbedo albedo also matched well with MODIS data partly because it used the MODIS surface anisotropy product in the gap-filling postprocess to generate a spatially complete data set. This gap-filling, however, may cause some uncertainties for events such as ephemeral snow and short-term drought. The overestimation of GlobAlbedo at high-latitude winters has been attributed to the difficulty in snow detection [*Muller*, 2013].

The constant-AOD setting for CLARA-SAL may have underestimated the AOD in tropical areas, which likely has resulted in the overestimation of surface albedo. In addition, CLARA-SAL provides the temporal-averaged albedo on a monthly basis using the instantaneous albedo values while most of the other satellite albedo products are normalized to the local solar noon. Therefore, it is possible that CLARA-SAL may have an overestimation of surface albedo compared with other satellite products. The magnitude of albedo bias from this angular normalization difference could be up to 0.009 and 4.3% according to *Jacob and Olioso* [2005]. However, the impacts of changes in the actual illumination angles due to orbital drift on the CLARA-SAL albedo are still needed for further analysis.

Although with a coarse spatial resolution of 2.5°, the ERBE data matched quite well with other data set in the middle- to low-latitude regions. The ERBE data have the constant-AOD setting similar to the one used for

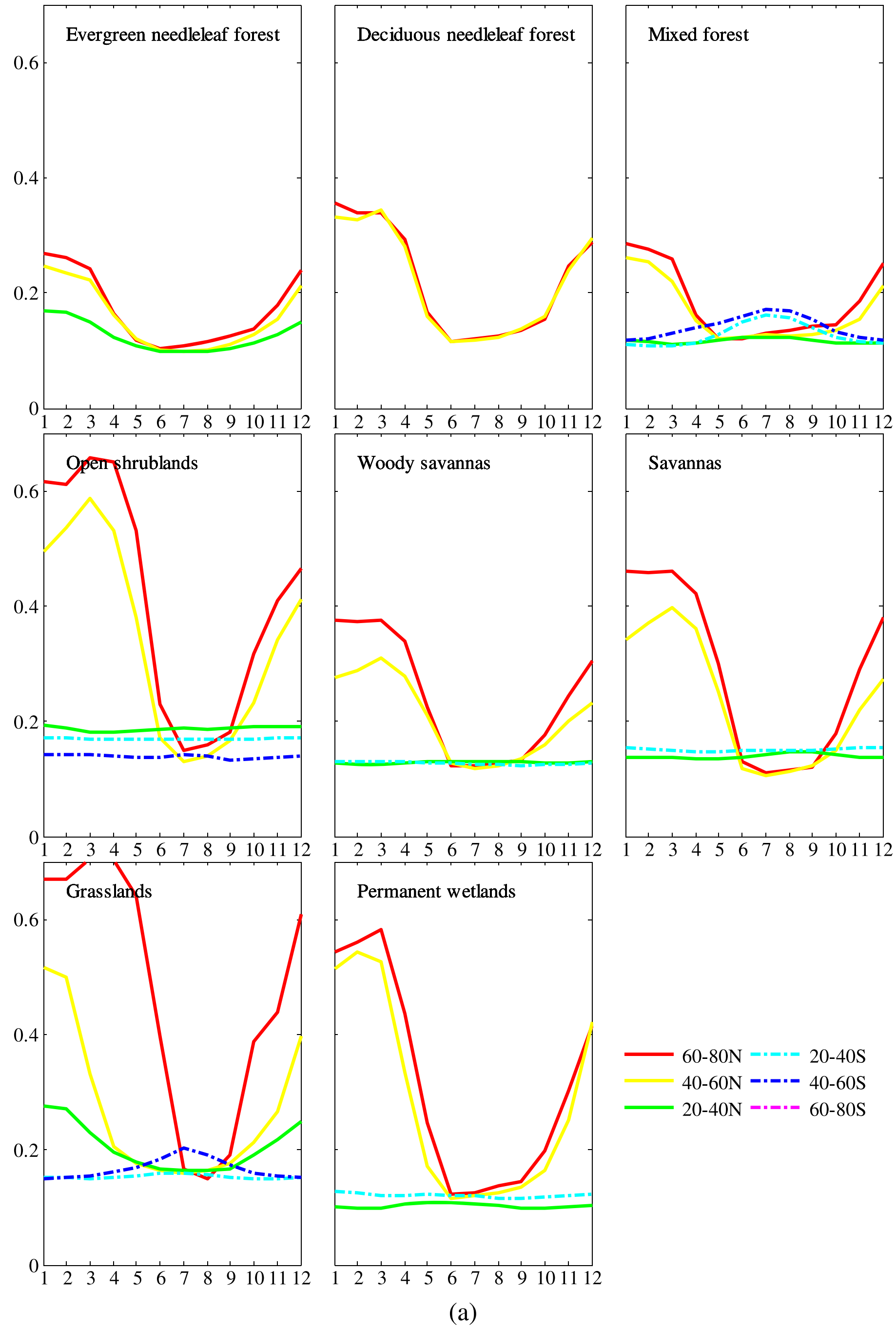

Figure 5. (a) Monthly averages and (b) SDs of albedo climatologies at different latitudinal zones, derived from MODIS, GLASS, and GlobAlbedo products for eight PFTs. *X* axis represents the month; *y* axis represents the surface albedo.

the CLARA-SAL data, which probably leads to the slight overestimation of surface albedo in some tropical regions and desert areas [*Jin et al*., 2003]. The coarse resolution of the broadband ERBE sensors reduces the capability in cloud identification (particularly in distinguishing snow/ice and cloud) [*Li and Leighton*, 1991], which is likely the reason for the underestimation of surface albedo over the latitudes higher than 50°N.

3.1.3. Albedo Climatology and PFTs

Albedo climatologies of PFTs have been widely used as reference or constraint in climate modeling studies [e.g., *Gao et al*., 2005]. However, accurate and fine-resolution PFT data for periods before the year 2000 have not yet been made available. We generated a multiyear stable land cover map (Figure 4) from the annual

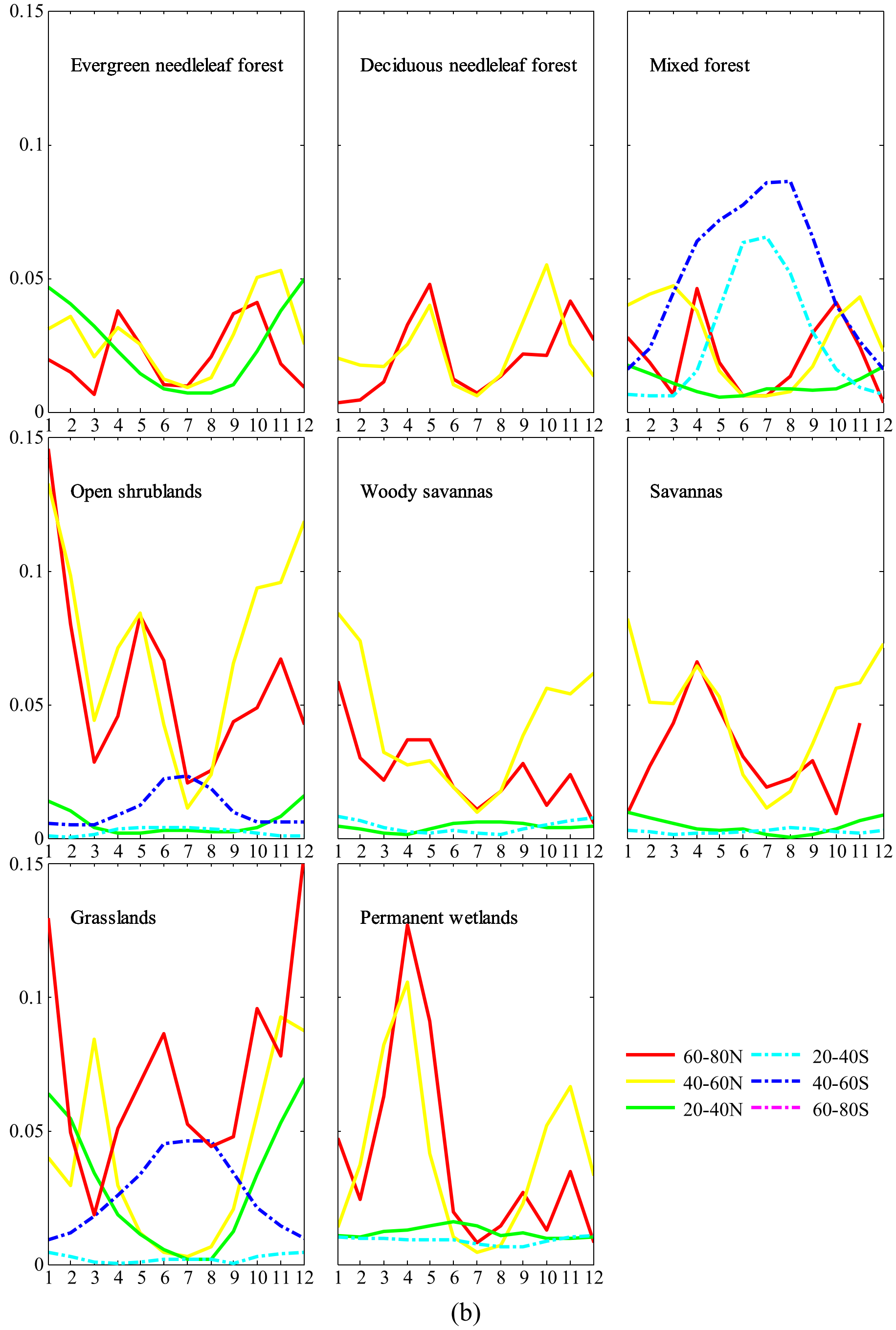

Figure 5. (continued)

MODIS land cover data (MCD12C1) and used it to build albedo climatologies for each of the PFTs during the period 2001–2010 for three satellite albedo products: GLASS, GlobAlbedo, and MODIS. Averages and SDs of these three products are shown in Figure 5. These three products were chosen because of their fine resolution, matching to that of the MODIS land cover data used.

For most of the PFTs between 40°N and 40°S, results show that climatological surface albedo values do not change much across seasons (Figures 5a and S1a) and that the different satellite albedo products agree very well (Figures 5b and S1b) for different seasons, except for the difference from October to April over the mixed forests in the Andes Mountains between 20°S and 40°S, which is a variably snow-covered region. In other words, the built albedo climatologies may be confidently used in climate models, in the region between 40°N

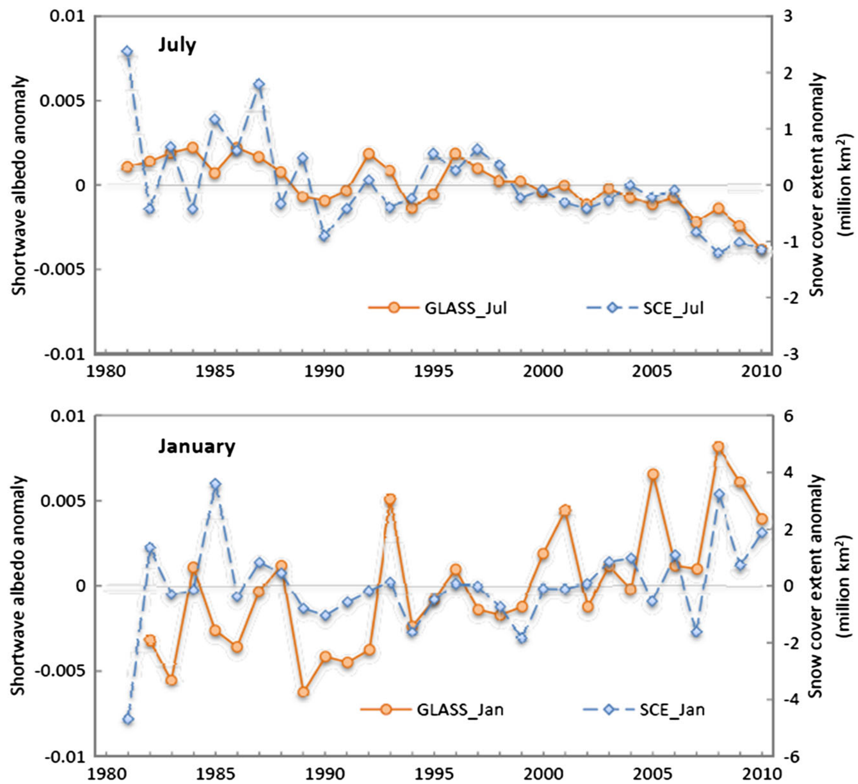

Figure 6. Surface albedo anomalies for the Northern Hemisphere in July and January, from the GLASS albedo product and snow cover extent anomalies for 1981–2010. CLARA-SAL, GEWEX, and ISCCP data were not shown here because of their larger annual variations.

and 40°S. Data in the zones 20°N–20°S are not plotted because they have small seasonal variations, and the differences among those three data sets are very small (<0.01).

The magnitude of seasonal albedo variation is much larger for middle to high latitudes, mainly because snowfall and snowmelt can significantly affect surface reflectivity. Plant phenology and soil moisture also contribute to the differences in this variation at different latitudes [*Gao et al*., 2005]. The effects of snow vary over the different PFTs [*Gao et al*., 2005; *Wu et al*., 2012]. The pixels with sparse vegetation cover (e.g., shrub and grass) tend to have much higher surface albedos than densely vegetated pixels (e.g., forest) in high-latitude winters. In addition, snow masking showed stronger impacts on pixels covered by sparse vegetation than those densely vegetated. Snow effects not only contribute to changes in surface albedo but also result in differences between satellite albedo products. The albedo differences for middle to high latitudes shown in Figure 3 can be largely attributed to differences between the shrub, grass, and crop albedos. There are two possible explanations for this. First, albedo algorithms are less reliable during snowy conditions when the solar zenith angle is large, due to theoretical limitations. Second, different temporal compositing strategies have been implemented in the generation of the satellite albedo products, which leads to differences in albedo, particularly during transition periods (e.g., during snowfall and snowmelt).

3.2. Spatial and Temporal Variation in Surface Albedo From Satellite-Based Data Sets

In this study, four global albedo data sets, namely, CLARA-SAL, GEWEX, GLASS, and ISCCP that nearly cover the past three decades 1981–2010 were selected to test the relationship of changes in surface albedo and snow cover for the Northern Hemisphere. We found that the July surface albedo decreased at a rate of 0.0013 decade^{-1} ($p < 0.01$) using the GLASS albedo product (Figure 6). With much larger interannual variations, the GEWEX and ISCCP albedos showed similar decreasing trends in albedo of 0.0053 decade^{-1} ($p = 0.06$) and 0.0086 decade^{-1} ($p < 0.01$), respectively (not shown). The July surface albedo trend from CLARA-SAL is not statistically significant. Hand in hand with the surface albedo decrease, the snow cover

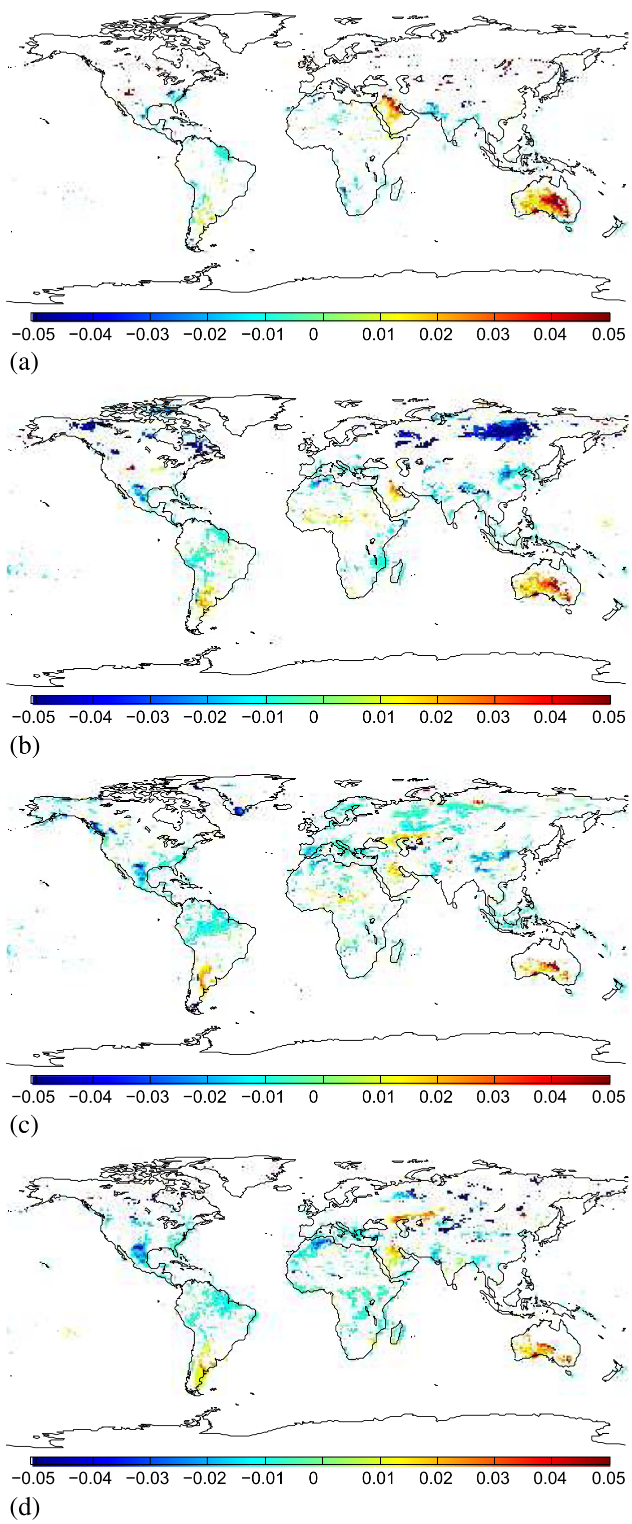

Figure 7. Decadal surface albedo trend derived from GLASS products (2000–2010) for (a) December–February, (b) Mar–May, (c) June–August, and (d) September–November. Trend is statistically significant at the 95% confidence level. Trend is not calculated over the Antarctica.

extent (SCE) [*Brown and Robinson*, 2011] decreased at a rate of 5.46×10^5 km^2 decade^{-1} ($p < 0.01$) (Figure 6). The correlation coefficient between GLASS surface albedo anomalies and SCE anomalies (taking the year of 2000 data as a reference) was 0.61 ($p < 0.01$) for the whole time period; it increased to 0.77 ($p < 0.01$) for the period of 2000–2010, as data after 2000 were believed to have improved sensitivity to surface changes particularly during transition periods over snow surfaces [*He et al*., 2013]. Positive correlation with SCE anomalies was also found using GEWEX and ISCCP with respective correlations of 0.33 ($p = 0.12$) and 0.50 ($p < 0.05$), whereas correlation was hardly found between anomalies in SCE and CLARA-SAL albedos. This positive correlation indicates that the SCE anomalies are likely to have been related to surface albedo anomalies during the past three decades. Moreover, it is likely that change in SCE is a driver of change in surface albedo. However, uncertainty in the SCE data [*Brown et al*., 2010; *Brown and Robinson*, 2011] may reduce its correlation with surface albedo as found in this study. Besides the SCE decrease, changes in snow morphology have been reported to be able to contribute approximately one third of the changes in snow albedo based on model simulations [*X Qu and Hall*, 2007], which, however, is currently difficult to be accurately quantified by remote sensing data on a global basis. In addition, since the CLARA-SAL and GLASS products used observations from AVHRR sensors, it is possible that uncertainties in the intercalibration for corrections on spectral response, sensor degradation, and orbital drift [*Heidinger et al*., 2010; *Molling et al*., 2010] can result in artifacts in surface albedo estimation, which further leads to the nonsignificant trend in surface albedo from CLARA-SAL during 1982–2009 and GLASS during 1981–2000, respectively.

We also found that for the Northern Hemisphere, surface albedo in winter changed in a direction opposite to that observed in summer (Figure 6). Satellite-based data sets from GLASS, CLARA-SAL, GEWEX, and ISCCP showed an increase in surface albedo at a rate of 0.0029 decade^{-1} ($p < 0.01$), 0.0002 decade^{-1} ($p = 0.92$), 0.0047 decade^{-1} ($p = 0.29$), and 0.00003 decade^{-1} ($p = 0.99$), respectively. Only the GLASS data showed a statistically significant trend at 95% confidence level. At the same time, SCE increased by 4.4×10^5 km^2 decade^{-1} ($p = 0.18$) (Figure 6). The correlation between anomalies from the GLASS albedo product and SCE is 0.44 ($p < 0.1$), which increased to 0.56 ($p < 0.1$) when only the data for the period of 2000–2010 were used. The correlation with SCE anomalies for GEWEX, ISCCP, and CLARA-SAL are 0.17 ($p = 0.42$), 0.44 ($p < 0.05$), and 0.17 ($p = 0.37$), respectively. One possible reason for this relationship is that disappearance of Arctic sea ice in recent decades due to global warming increased atmospheric water vapor content in winter and consequently more and/or heavier snowfall on land surface in winter in the northern latitudes [*Liu et al*., 2012]. Compared with the relatively larger correlation in July, the decreased sensitivity of satellite albedo to SCE changes in January can result from the reduced spatial coverage at high latitudes in winter and the differences in satellite albedo data processing add uncertainty in this analysis. Due to the limitations of satellite albedo products in high northern latitudes in winter (Figure 3), further efforts are urged to investigate the reason of the albedo's decreasing trend and poor correlation of satellite albedo and SCE.

Temporal trends in surface albedo vary from place to place. Figure 7 shows the trend of surface albedo during 2000–2010. Climate change has resulted in early snowmelt and/or vegetation onset over boreal areas [*Maignan et al*., 2008], which may have caused the dramatic decrease in surface albedo, particularly over forest areas in early spring (Figure 7). In addition, a significant albedo decrease (>0.05 decade^{-1}) in early spring in northern Russia was found in this study, which was due to the snow masking effects of vegetation [*Loranty et al*., 2014]; this can be attributed to the northward expansion of the boreal forest in the northern tundra area in Russia, which has resulted from the recent climate warming [*MacDonald et al*., 2008]. A decreasing summer land surface albedo has been found in the Greenland ice sheet since the 1980s [*He et al*., 2013]. Although the extent of the albedo-decreasing area is not quite significant, as shown in Figure 7, its associated snow/ice albedo feedback with the adjacent sea ice area could bring amplified effects to global climate change.

Observed changes in surface albedo may also be the result of soil moisture changes, especially in semiarid areas. It was found by *Dorigo et al*. [2012] that observed albedo decrease and increase in southwest Africa and central to west Australia could be largely explained by soil moisture increase and decrease, respectively (particularly from March to May). Major soil moisture variations are mainly precipitation driven, especially in moisture-limited areas [*Dorigo et al*., 2012; *Jung et al*., 2010]. If a drier condition becomes more frequent and/or extensive in the future, which leads to soil moisture decrease [*Sherwood and Fu*, 2014], vegetation cover may decrease accompanied by increase in surface albedo. This may result in reduced evapotranspiration and further contribute to the decrease in precipitation, which will in turn exacerbate the drought condition.

4. Conclusions

Surface albedo is a key factor in climate models, as it regulates Earth's surface energy budget. However, the effect of anthropogenic impacts on land surface albedo change is still quite uncertain in the Intergovernmental Panel on Climate Change's Fourth Assessment Report. Multiple long-term global land surface albedo data sets have recently become available, which enables systematic assessments of albedo climatology and trends derived from satellite observations. In this study, we focused on the global albedo climatology, and we compared and assessed multiple satellite-based albedo data sets for the period 1981–2010 at the global scale.

Major findings of this study include the following:

1. Most of the satellite-based albedo data sets can achieve an agreement within a difference of approximately 0.02–0.03 in climatological albedo values on a global basis. This promises a great potential to apply the climatological surface albedo data derived from satellite observations in validating, calibrating, and further improving surface albedo simulations and parameterizations in current climate models. However, in general, ISCCP is most likely to have underestimated surface albedo for May–September. Underestimation was also identified in GEWEX data for October–May in the Northern Hemisphere. Albedo differences remain quite large for early spring (February–April) in the Northern Hemisphere, which was likely the result of differences in snow detection among the data sets and requires more detailed investigations. CLARA-SAL showed a constant overestimation in all seasons. Data sets at finer resolutions such as GLASS,

MODIS, MERIS, and GlobAlbedo data showed better agreement with the multidata mean values on a global basis, while GlobAlbedo overestimated surface albedo in northern winters.

2. How well the investigated satellite-based albedo data sets agree on surface albedo strongly depends on latitude. Except for ISCCP and GEWEX data, the satellite albedo data sets are in a better agreement for summer albedo estimation at all latitudes, whereas these data sets generally do not agree on winter albedo, particularly at high latitudes. The constant-AOD settings have led to the overestimation of surface albedo in CLARA-SAL and ERBE data over some tropical and desert regions; the albedo biases can be reduced by using a location-dependent AOD climatology in the retrieving process. From the three fine-resolution (0.05°) data sets, a high level of consistency was found for all the PFTs in middle to low latitudes. Large spread was identified for albedo estimations at middle to high latitudes, particularly for the PFTs with mixed cover of sparse vegetation and snow in winter and early spring including open shrubland, mixed forest, grassland, and wetlands, where drought may also contribute to the uncertainty of albedo estimation. Further efforts are needed to better understand this inconsistency and to improve the satellite-based albedo estimation.
3. Satellite-based surface albedo and SCE were found to be highly correlated, which indicates that snow cover change is a major driver of surface albedo change and albedo change can in turn result in snow cover change in the Northern Hemisphere, particularly in summer. For a more accurate detection of albedo trends in decadal time series, it is important that albedo variation is accurately analyzed. Therefore, climate model parameterizations of snow cover and snow albedo need to be improved [*Brovkin et al*., 2013; *Brutel-Vuilmet et al*., 2013; *Fletcher et al*., 2012; *He et al*., 2013; *Qu and Hall*, 2013].

Requirements on albedo accuracy have generally transitioned to be more specific on the application period and location as a result of the advances in modeling techniques in recent decades [e.g., *Loew et al*., 2014; *Wang et al*., 2007; *Widlowski et al*., 2011]. In-depth investigation is required to better understand the differences between satellite-based albedo data sets at regional scale, based on which suggestions for data selection can be made according to the specific needs of applications. Nevertheless, more accurate estimation of surface albedo could improve our understanding of surface radiative forcing and snow albedo feedback and their long-term effects on climate [*Flanner et al*., 2011]. Unfortunately, the level of inconsistency between albedo data sets at high latitudes is still very high, which leads to the wide spread in snow albedo feedback estimations [*Colman*, 2013; *Dessler*, 2013; *Soden et al*., 2008]. Based on an improved understanding on the origination of the albedo differences, a more accurate long-term global albedo data set can be derived to resolve observed inconsistencies, relying on the recent techniques of data fusion [e.g., *He et al*., 2014b]. In addition, more accurate land surface albedo data could allow for a more accurate assessment of important anthropogenic impacts such as land cover and land use change on global/regional climate. This could in turn allow policymakers to design mitigation strategies that are not limited to carbon-induced climate change alone.

Acknowledgments
We thank the relevant teams and organizations for providing the data sets used in this study. The GLASS albedo product is provided by Beijing Normal University and available at http://glass-product.bnu.edu.cn/en/ and http://glcf.umd.edu/data/abd/. The MODIS albedo and land cover products are processed and available at NASA Land Processes Distributed Active Archive Center (LP DAAC). The CERES EBAF and GEWEX SRB data are maintained by NASA Langley Research Center Atmospheric Science Data Center (ASDC). The ISCCP data are provided by the NASA Goddard Institute for Space Studies (GISS). The MERRA reanalysis data are from the NASA Modeling and Assimilation Data and Information Services Center (MDISC). The GlobAlbedo product was obtained from the European Space Agency (ESA) GlobAlbedo product downloaded from http://www.GlobAlbedo.org. The CLARA-SAL product is provided by the Satellite Application Facility on Climate Monitoring (CM SAF) and available at http://wui.cmsaf.eu. The ERBE albedo product is provided by Zhanqing Li from the University of Maryland. The NCEP reanalysis climatology data are provided by the National Oceanic and Atmospheric Administration's (NOAA) Earth System Research Laboratory (ESRL) Physical Sciences Division (PSD). The SCE data were obtained from the Rutgers University Global Snow Lab. We would also like to thank the three anonymous reviewers for their valuable comments and suggestions.

References

Brovkin, V., L. Boysen, T. Raddatz, V. Gayler, A. Loew, and M. Claussen (2013), Evaluation of vegetation cover and land-surface albedo in MPI-ESM CMIP5 simulations, *J. Adv. Model. Earth Syst.*, *5*(1), 48–57, doi:10.1029/2012MS000169.

Brown, R. D., and D. A. Robinson (2011), Northern Hemisphere spring snow cover variability and change over 1922–2010 including an assessment of uncertainty, *Cryosphere*, *5*(1), 219–229, doi:10.5194/tc-5-219-2011.

Brown, R. D., C. Derksen, and L. B. Wang (2010), A multi-data set analysis of variability and change in Arctic spring snow cover extent, 1967–2008, *J. Geophys. Res.*, *115*, D16111, doi:10.1029/2010JD013975.

Brutel-Vuilmet, C., M. Menegoz, and G. Krinner (2013), An analysis of present and future seasonal Northern Hemisphere land snow cover simulated by CMIP5 coupled climate models, *Cryosphere*, *7*(1), 67–80, doi:10.5194/tc-7-67-2013.

Cescatti, A., et al. (2012), Intercomparison of MODIS albedo retrievals and in situ measurements across the global FLUXNET network, *Remote Sens. Environ.*, *121*, 323–334, doi:10.1016/j.rse.2012.02.019.

Colman, R. A. (2013), Surface albedo feedbacks from climate variability and change, *J. Geophys. Res. Atmos.*, *118*, 2827–2834, doi:10.1002/jgrd.50230.

Csiszar, I., and G. Gutman (1999), Mapping global land surface albedo from NOAA AVHRR, *J. Geophys. Res.*, *104*(D6), 6215–6228, doi:10.1029/1998JD200090.

Davidson, A., and S. Wang (2005), Spatiotemporal variations in land surface albedo across Canada from MODIS observations, *Can. J. Remote Sens.*, *31*(5), 377–390.

Dessler, A. E. (2013), Observations of climate feedbacks over 2000–10 and comparisons to climate models, *J. Clim.*, *26*(1), 333–342, doi:10.1175/Jcli-D-11-00640.1.

Dorigo, W., R. de Jeu, D. Chung, R. Parinussa, Y. Liu, W. Wagner, and D. Fernandez-Prieto (2012), Evaluating global trends (1988–2010) in harmonized multi-satellite surface soil moisture, *Geophys. Res. Lett.*, *39*, L18405, doi:10.1029/2012GL052988.

Dozier, J., R. J. Barry, K. M. Jezek, R. H. Thomas, and J. Vesecky (1989), *Prospects and Concerns for Satellite Remote Sensing of Snow and Ice*, 55 pp., National Academy Press, Washington, D. C.

Fang, H. L., S. L. Liang, H. Y. Kim, J. R. Townshend, C. L. Schaaf, A. H. Strahler, and R. E. Dickinson (2007), Developing a spatially continuous 1 km surface albedo data set over North America from Terra MODIS products, *J. Geophys. Res.*, *112*, D20206, doi:10.1029/2006JD008377.

Fischer, J., R. Preusker, J. Muller, and M. Zuhlke (2009), ALBEDOMAP-Validation Report. [Available at http://www.brockmann-consult.de/albedomap/pdf/MERIS-AlbedoMap-Validation-1.0.pdf.]

Flanner, M. G., K. M. Shell, M. Barlage, D. K. Perovich, and M. A. Tschudi (2011), Radiative forcing and albedo feedback from the Northern Hemisphere cryosphere between 1979 and 2008, *Nat. Geosci.*, *4*(3), 151–155.

Fletcher, C. G., H. X. Zhao, P. J. Kushner, and R. Fernandes (2012), Using models and satellite observations to evaluate the strength of snow albedo feedback, *J. Geophys. Res.*, *117*, D11117, doi:10.1029/2012JD017724.

Gao, F., C. B. Schaaf, A. H. Strahler, A. Roesch, W. Lucht, and R. Dickinson (2005), MODIS bidirectional reflectance distribution function and albedo Climate Modeling Grid products and the variability of albedo for major global vegetation types, *J. Geophys. Res.*, *110*, D01104, doi:10.1029/2004JD005190.

Govaerts, Y., and A. Lattanzio (2008), Estimation of surface albedo increase during the eighties Sahel drought from Meteosat observations, *Global Planet. Change*, *64*(3–4), 139–145, doi:10.1016/j.gloplacha.2008.04.004.

Govaerts, Y., B. Pinty, M. Taberner, and A. Lattanzio (2006), Spectral conversion of surface albedo derived from meteosat first generation observations, *IEEE Geosci. Remote Sens. Lett.*, *3*(1), 23–27, doi:10.1109/Lgrs.2005.854202.

Gui, S., S. L. Liang, K. C. Wang, L. Li, and X. T. Zhang (2010), Assessment of three satellite-estimated land surface downwelling shortwave irradiance data sets, *IEEE Geosci. Remote Sens. Lett.*, *7*(4), 776–780, doi:10.1109/lgrs.2010.2048196.

Hansen, J., and L. Nazarenko (2004), Soot climate forcing via snow and ice albedos, *Proc. Natl. Acad. Sci. U.S.A.*, *101*(2), 423–428, doi:10.1073/pnas.2237157100.

He, T., S. L. Liang, D. Wang, H. Wu, Y. Yu, and J. Wang (2012), Estimation of surface albedo and directional reflectance from Moderate Resolution Imaging Spectroradiometer (MODIS) observations, *Remote Sens. Environ.*, *119*, 286–300, doi:10.1016/j.rse.2012.01.004.

He, T., S. L. Liang, Y. Yu, D. Wang, F. Gao, and Q. Liu (2013), Greenland surface albedo changes in July 1981–2012 from satellite observations, *Environ. Res. Lett.*, *8*(4, 044043), doi:10.1088/1748-9326/8/4/044043.

He, T., S. L. Liang, D. Wang, Q. Shi, and X. Tao (2014a), Estimation of high-resolution land surface shortwave albedo from AVIRIS data, *IEEE J. Sel. Top. Appl. Earth Obs. Remote Sens.*, *7*, doi:10.1109/JSTARS.2014.2302234, in press.

He, T., S. L. Liang, D. Wang, Y. Shuai, and Y. Yu (2014b), Fusion of satellite land surface albedo products across scales using a multiresolution tree method in the north central United States, *IEEE Trans. Geosci. Remote Sens.*, *52*(6), 3428–3439, doi:10.1109/tgrs.2013.2272935.

Heidinger, A. K., W. C. Straka, C. C. Molling, J. T. Sullivan, and X. Q. Wu (2010), Deriving an inter-sensor consistent calibration for the AVHRR solar reflectance data record, *Int. J. Remote Sens.*, *31*(24), 6493–6517, doi:10.1080/01431161.2010.496472.

Hudson, S. R., S. G. Warren, and S. Kato (2010), A comparison of shortwave reflectance over the East Antarctic Plateau observed by CERES to that estimated from surface reflectance observations, *J. Geophys. Res.*, *115*, D20110, doi:10.1029/2010JD013912.

Jacob, F., and A. Olioso (2005), Derivation of diurnal courses of albedo and reflected solar irradiance from airborne POLDER data acquired near solar noon, *J. Geophys. Res.*, *110*, D10104, doi:10.1029/2004JD004888.

Jeong, S. J., C. H. Ho, H. J. Gim, and M. E. Brown (2011), Phenology shifts at start vs. end of growing season in temperate vegetation over the Northern Hemisphere for the period 1982–2008, *Global Change Biology*, *17*(7), 2385–2399, doi:10.1111/j.1365-2486.2011.02397.x.

Jin, Y. F., C. B. Schaaf, C. E. Woodcock, F. Gao, X. W. Li, A. H. Strahler, W. Lucht, and S. L. Liang (2003), Consistency of MODIS surface bidirectional reflectance distribution function and albedo retrievals: 2. Validation, *J. Geophys. Res.*, *108*(D5), 4159, doi:10.1029/2002JD002804.

Jung, M., et al. (2010), Recent decline in the global land evapotranspiration trend due to limited moisture supply, *Nature*, *467*(7318), 951–954, doi:10.1038/nature09396.

Kalnay, E., et al. (1996), The NCEP/NCAR 40-year reanalysis project, *Bull. Am. Meteorol. Soc.*, *77*(3), 437–471, doi:10.1175/1520-0477(1996)077<0437:tnyrp>2.0.co;2.

Karlsson, K. G., et al. (2013), CLARA-A1: A cloud, albedo, and radiation dataset from 28 yr of global AVHRR data, *Atmos. Chem. Phys.*, *13*(10), 5351–5367, doi:10.5194/acp-13-5351-2013.

Kato, S., N. G. Loeb, F. G. Rose, D. R. Doelling, D. A. Rutan, T. E. Caldwell, L. S. Yu, and R. A. Weller (2013), Surface irradiances consistent with CERES-derived top-of-atmosphere shortwave and longwave irradiances, *J. Clim.*, *26*(9), 2719–2740, doi:10.1175/Jcli-D-12-00436.1.

Lewis, P., et al. (2013), GlobAlbedo: Algorithm theoretical basis document (V4.12).

Li, Z. Q., and L. Garand (1994), Estimation of surface albedo from space—A parameterization for global application, *J. Geophys. Res.*, *99*(D4), 8335–8350, doi:10.1029/94JD00225.

Li, Z. Q., and H. G. Leighton (1991), Scene identification and its effect on cloud radiative forcing in the arctic, *J. Geophys. Res.*, *96*(D5), 9175–9188, doi:10.1029/91JD00529.

Liang, S. L. (2001), Narrowband to broadband conversions of land surface albedo I Algorithms, *Remote Sens. Environ.*, *76*(2), 213–238, doi:10.1016/s0034-4257(00)00205-4.

Liang, S. L., K. C. Wang, X. T. Zhang, and M. Wild (2010), Review on estimation of land surface radiation and energy budgets from ground measurement, remote sensing and model simulations, *IEEE J. Sel. Top. Appl. Earth Obs. Remote Sens.*, *3*(3), 225–240, doi:10.1109/jstars.2010.2048556.

Liang, S. L., X. Li, and J. Wang (Eds) (2012), *Advanced Remote Sensing: Terrestrial Information Extraction and Applications*, Academic Press, Oxford, U. K.

Liang, S. L., X. T. Zhang, T. He, J. Cheng, and D. Wang (2013a), Remote sensing of the land surface radiation budget, in *Remote Sensing of Energy Fluxes and Soil Moisture Content*, pp. 121–162, CRC Press, Boca Raton, Fla., doi:10.1201/b15610-7.

Liang, S. L., et al. (2013b), A long-term Global LAnd Surface Satellite (GLASS) data-set for environmental studies, *Int. J. Digital Earth*, *6*(sup1), 5–33, doi:10.1080/17538947.2013.805262.

Liu, J. C., C. Schaaf, A. Strahler, Z. T. Jiao, Y. M. Shuai, Q. L. Zhang, M. Roman, J. A. Augustine, and E. G. Dutton (2009), Validation of Moderate Resolution Imaging Spectroradiometer (MODIS) albedo retrieval algorithm: Dependence of albedo on solar zenith angle, *J. Geophys. Res.*, *114*, D01106, doi:10.1029/2008JD009969.

Liu, J., J. A. Curry, H. Wang, M. Song, and R. M. Horton (2012), Impact of declining Arctic sea ice on winter snowfall, *Proc. Natl. Acad. Sci. U.S.A.*, *109*(11), 4074–4079, doi:10.1073/pnas.1114910109.

Liu, N. F., Q. Liu, L. Z. Wang, S. L. Liang, J. G. Wen, Y. Qu, and S. H. Liu (2013a), A statistics-based temporal filter algorithm to map spatiotemporally continuous shortwave albedo from MODIS data, *Hydrol. Earth Syst. Sci.*, *17*(6), 2121–2129, doi:10.5194/hess-17-2121-2013.

Liu, Q., L. Wang, Y. Qu, N. Liu, S. Liu, H. Tang, and S. Liang (2013b), Preliminary evaluation of the long-term GLASS albedo product, *Int. J. Digital Earth*, *6*, 69–95, doi:10.1080/17538947.2013.804601.

Loarie, S. R., D. B. Lobell, G. P. Asner, Q. Z. Mu, and C. B. Field (2011), Direct impacts on local climate of sugar-cane expansion in Brazil, *Nat. Clim. Change*, *1*(2), 105–109.

Loew, A., and Y. Govaerts (2010), Towards multidecadal consistent Meteosat surface albedo time series, *Remote Sens.*, *2*(4), 957–967, doi:10.3390/rs2040957.

Loew, A., P. M. van Bodegom, J. L. Widlowski, J. Otto, T. Quaife, B. Pinty, and T. Raddatz (2014), Do we (need to) care about canopy radiation schemes in DGVMs? Caveats and potential impacts, *Biogeosciences*, *11*(7), 1873–1897, doi:10.5194/bg-11-1873-2014.

Loranty, M. M., L. T. Berner, S. J. Goetz, Y. F. Jin, and J. T. Randerson (2014), Vegetation controls on northern high latitude snow-albedo feedback: Observations and CMIP5 model simulations, *Global Change Biology*, *20*(2), 594–606, doi:10.1111/Gcb.12391.

Lyons, E. A., Y. F. Jin, and J. T. Randerson (2008), Changes in surface albedo after fire in boreal forest ecosystems of interior Alaska assessed using MODIS satellite observations, *J. Geophys. Res.*, *113*, G02012, doi:10.1029/2007JG000606.

MacDonald, G. M., K. V. Kremenetski, and D. W. Beilman (2008), Climate change and the northern Russian treeline zone, *Philos. Trans. R. Soc. London, Ser. B*, *363*(1501), 2285–2299, doi:10.1098/rstb.2007.2200.

Maignan, F., F. M. Breon, and R. Lacaze (2004), Bidirectional reflectance of Earth targets: Evaluation of analytical models using a large set of spaceborne measurements with emphasis on the Hot Spot, *Remote Sens. Environ.*, *90*(2), 210–220, doi:10.1016/j.rse.2003.12.006.

Maignan, F., F. M. Breon, E. Vermote, P. Ciais, and N. Viovy (2008), Mild winter and spring 2007 over western Europe led to a widespread early vegetation onset, *Geophys. Res. Lett.*, *35*, L02404, doi:10.1029/2007GL032472.

Martonchik, J. V., D. J. Diner, B. Pinty, M. M. Verstraete, R. B. Myneni, Y. Knyazikhin, and H. R. Gordon (1998), Determination of land and ocean reflective, radiative, and biophysical properties using multiangle imaging, *IEEE Trans. Geosci. Remote Sens.*, *36*(4), 1266–1281, doi:10.1109/36.701077.

Molling, C. C., A. K. Heidinger, W. C. Straka, and X. Q. Wu (2010), Calibrations for AVHRR channels 1 and 2: Review and path towards consensus, *Int. J. Remote Sens.*, *31*(24), 6519–6540, doi:10.1080/01431161.2010.496473.

Muller, J.-P. (2013), GlobAlbedo final validation reportRep., University College London. [Available at http://www.globalbedo.org/docs/GlobAlbedo_FVR_V1_2_web.pdf.]

Muller, J.-P., et al. (2012), The ESA GlobAlbedo project for mapping the Earth's land surface albedo for 15 years from European sensors, paper presented at IEEE Geoscience and Remote Sensing Symposium (IGARSS) 2012, IEEE, Munich, Germany.

Offerle, B., P. Jonsson, I. Eliasson, and C. S. B. Grimmond (2005), Urban modification of the surface energy balance in the West African Sahel: Ouagadougou, Burkina Faso, *J. Clim.*, *18*(19), 3983–3995, doi:10.1175/jcli3520.1.

Oleson, K. W., G. B. Bonan, C. Schaaf, F. Gao, Y. F. Jin, and A. Strahler (2003), Assessment of global climate model land surface albedo using MODIS data, *Geophys. Res. Lett.*, *30*(8), 1443, doi:10.1029/2002GL016749.

Pedelty, J., et al. (2007), Generating a long-term land data record from the AVHRR and MODIS Instruments, paper presented at Geoscience and Remote Sensing Symposium, 2007. IGARSS 2007. IEEE International, 23–28 July.

Pinker, R. T., and I. Laszlo (1992), Modeling surface solar irradiance for satellite applications on a global scale, *J. Appl. Meteorol.*, *31*(2), 194–211, doi:10.1175/1520-0450(1992)031<0194:mssifs>2.0.co;2.

Pinty, B., F. Roveda, M. M. Verstraete, N. Gobron, Y. Govaerts, J. V. Martonchik, D. J. Diner, and R. A. Kahn (2000), Surface albedo retrieval from Meteosat: 1. Theory, *J. Geophys. Res.*, *105*(D14), 18,099–18,112, doi:10.1029/2000JD900113.

Pinty, B., A. Lattanzio, J. V. Martonchik, M. M. Verstraete, N. Gobron, M. Taberner, J. L. Widlowski, R. E. Dickinson, and Y. Govaerts (2005), Coupling diffuse sky radiation and surface albedo, *J. Atmos. Sci.*, *62*(7), 2580–2591, doi:10.1175/jas3479.1.

Popp, C., P. Wang, D. Brunner, P. Stammes, Y. Zhou, and M. Grzegorski (2011), MERIS albedo climatology for FRESCO + O-2 A-band cloud retrieval, *Atmos. Meas. Tech.*, *4*(3), 463–483, doi:10.5194/amt-4-463-2011.

Qin, J., K. Yang, S. L. Liang, H. Zhang, Y. M. Ma, X. F. Guo, and Z. Q. Chen (2011), Evaluation of surface albedo from GEWEX-SRB and ISCCP-FD data against validated MODIS product over the Tibetan Plateau, *J. Geophys. Res.*, *116*, D24116, doi:10.1029/2011JD015823.

Qu, X., and A. Hall (2007), What controls the strength of snow-albedo feedback?, *J. Clim.*, *20*(15), 3971–3981, doi:10.1175/jcli4186.1.

Qu, X., and A. Hall (2013), On the persistent spread in snow-albedo feedback, *Clim. Dyn.*, *42*(1-2), 69, doi:10.1007/s00382-013-1774-0.

Qu, Y., Q. Liu, S. Liang, L. Wang, N. Liu, and S. Liu (2014), Direct-estimation algorithm for mapping daily land-surface broadband albedo from MODIS data, *IEEE Trans. Geosci. Remote Sens.*, *52*(2), 907–901, doi:10.1109/tgrs.2013.2245670.

Rahman, H., and G. Dedieu (1994), SMAC—A simplified method for the atmospheric correction of satellite measurements in the solar spectrum, *Int. J. Remote Sens.*, *15*(1), 123–143.

Rienecker, M. M., et al. (2011), MERRA: NASA's Modern-Era retrospective analysis for research and applications, *J. Clim.*, *24*(14), 3624–3648, doi:10.1175/jcli-d-11-00015.1.

Riihela, A., T. Manninen, V. Laine, K. Andersson, and F. Kaspar (2013), CLARA-SAL: A global 28 yr timeseries of Earth's black-sky surface albedo, *Atmos. Chem. Phys.*, *13*(7), 3743–3762, doi:10.5194/acp-13-3743-2013.

Roman, M. O., C. B. Schaaf, P. Lewis, F. Gao, G. P. Anderson, J. L. Privette, A. H. Strahler, C. E. Woodcock, and M. Barnsley (2010), Assessing the coupling between surface albedo derived from MODIS and the fraction of diffuse skylight over spatially-characterized landscapes, *Remote Sens. Environ.*, *114*(4), 738–760, doi:10.1016/j.rse.2009.11.014.

Roman, M. O., C. K. Gatebe, Y. Shuai, Z. Wang, F. Gao, J. G. Masek, T. He, S. Liang, and C. B. Schaaf (2013), Use of in situ and airborne multiangle data to assess MODIS- and Landsat-based estimates of directional reflectance and albedo, *IEEE Trans. Geosci. Remote Sens.*, *51*(3), 1393–1404, doi:10.1109/TGRS.2013.2243457.

Rutan, D., F. Rose, M. Roman, N. Manalo-Smith, C. Schaaf, and T. Charlock (2009), Development and assessment of broadband surface albedo from Clouds and the Earth's Radiant Energy System Clouds and Radiation Swath data product, *J. Geophys. Res.*, *114*, D08125, doi:10.1029/2008JD010669.

Schaaf, C. B., et al. (2002), First operational BRDF, albedo nadir reflectance products from MODIS, *Remote Sens. Environ.*, *83*(1–2), 135–148.

Sellers, P. J., et al. (1995), Remote sensing of the land surface for studies of global change—Models, algorithms, experiments, *Remote Sens. Environ.*, *51*(1), 3–26.

Sherwood, S., and Q. Fu (2014), A drier future?, *Science*, *343*(6172), 737–739, doi:10.1126/science.1247620.

Shi, Q., and S. Liang (2013), Characterizing the surface radiation budget over the Tibetan Plateau with ground-measured, reanalysis, and remote sensing datasets. Part 2: Spatiotemporal analysis, *J. Geophys. Res. Atmos.*, *118*, 8921–8934, doi:10.1002/jgrd.50719.

Shuai, Y. M., J. G. Masek, F. Gao, C. B. Schaaf, and T. He (2014), An approach for the long-term 30-m land surface snow-free albedo retrieval from historic Landsat surface reflectance and MODIS-based a priori anisotropy knowledge, *Remote Sens. Environ.*, *152*, 467–479, doi:10.1016/j.rse.2014.07.009.

Soden, B. J., I. M. Held, R. Colman, K. M. Shell, J. T. Kiehl, and C. A. Shields (2008), Quantifying climate feedbacks using radiative kernels, *J. Clim.*, *21*(14), 3504–3520, doi:10.1175/2007jcli2110.1.

Stackhouse, P. W., S. J. Cox, J. C. Mikovitz, W. B. Rossow, Y. C. Zhang, L. M. Hinkelman, R. T. Pinker, E. Raschke, and S. Kinne (2012), Chapter 4: Surface radiation budget, *Rep.*, World Climate Research Programme, NASA.

10.1002/2014JD021667

Stroeve, J., J. E. Box, F. Gao, S. L. Liang, A. Nolin, and C. Schaaf (2005), Accuracy assessment of the MODIS 16-day albedo product for snow: Comparisons with Greenland in situ measurements, *Remote Sens. Environ.*, *94*(1), 46–60, doi:10.1016/j.rse.2004.09.011.

Wang, D., S. L. Liang, T. He, and Y. Yu (2013), Direct estimation of land surface albedo from VIIRS data: Algorithm improvement and preliminary validation, *J. Geophys. Res. Atmos.*, *118*, 12,577–12,586, doi:10.1002/2013JD020417.

Wang, S., and A. Davidson (2007), Impact of climate variations on surface albedo of a temperate grassland, *Agric. For. Meteorol.*, *142*(2–4), 133–142, doi:10.1016/j.agrformet.2006.03.027.

Wang, S., A. P. Trishchenko, K. V. Khlopenkov, and A. Davidson (2006), Comparison of International Panel on Climate Change Fourth Assessment Report climate model simulations of surface albedo with satellite products over northern latitudes, *J. Geophys. Res.*, *111*, D21108, doi:10.1029/2005JD006728.

Wang, S., A. P. Trishchenko, and X. M. Sun (2007), Simulation of canopy radiation transfer and surface albedo in the EALCO model, *Clim. Dyn.*, *29*(6), 615–632, doi:10.1007/s00382-007-0252-y.

Wang, Z., and X. B. Zeng (2010), Evaluation of snow albedo in land models for weather and climate studies, *J. Appl. Meteorol. Climatol.*, *49*(3), 363–380, doi:10.1175/2009jamc2134.1.

Wang, Z., X. Zeng, M. Barlage, R. E. Dickinson, F. Gao, and C. B. Schaaf (2004), Using MODIS BRDF and albedo data to evaluate global model land surface albedo, *J. Hydrometeorol.*, *5*(1), 3–14, doi:10.1175/1525-7541(2004)005<0003:umbaad>2.0.co;2.

Wang, Z., C. B. Schaaf, M. J. Chopping, A. H. Strahler, J. Wang, M. O. Roman, A. V. Rocha, C. E. Woodcock, and Y. Shuai (2012), Evaluation of Moderate-resolution Imaging Spectroradiometer (MODIS) snow albedo product (MCD43A) over tundra, *Remote Sens. Environ.*, *117*, 264–280, doi:10.1016/j.rse.2011.10.002.

Widlowski, J. L., et al. (2011), RAMI4PILPS: An intercomparison of formulations for the partitioning of solar radiation in land surface models, *J. Geophys. Res.*, *116*, G02019, doi:10.1029/2010JG001511.

Wu, A. H., Z. Q. Li, and J. Cihlar (1995), Effects of land-cover type and greenness on advanced very high-resolution radiometer bidirectional reflectances: Analysis and removal, *J. Geophys. Res.*, *100*(D5), 9179–9192, doi:10.1029/95JD00512.

Wu, H., S. Liang, L. Tong, T. He, and Y. Yu (2012), Bidirectional reflectance for multiple snow-covered land types from MISR products, *IEEE Geosci. Remote Sens. Lett.*, *9*(5), 994–998, doi:10.1109/LGRS.2012.2187041.

Xiong, X. Z., K. Stamnes, and D. Lubin (2002), Surface albedo over the Arctic Ocean derived from AVHRR and its validation with SHEBA data, *J. Appl. Meteorol.*, *41*(4), 413–425, doi:10.1175/1520-0450(2002)041<0413:saotao>2.0.co;2.

Xu, B. Q., et al. (2009), Black soot and the survival of Tibetan glaciers, *Proc. Natl. Acad. Sci. U.S.A.*, *106*(52), 22,114–22,118, doi:10.1073/pnas.0910444106.

Zhang, X. T., S. L. Liang, K. C. Wang, L. Li, and S. Gui (2010), Analysis of global land surface shortwave broadband albedo from multiple data sources, *IEEE J. Sel. Top. Appl. Earth Obs. Remote Sens.*, *3*(3), 296–305, doi:10.1109/jstars.2010.2049342.

Zhang, Y. C., W. B. Rossow, and A. A. Lacis (1995), Calculation of surface and top of atmosphere radiative fluxes from physical quantities based on ISCCP data sets. 1. Method and sensitivity to input data uncertainties, *J. Geophys. Res.*, *100*(D1), 1149–1165, doi:10.1029/94JD02747.

Zhang, Y. C., W. B. Rossow, A. A. Lacis, V. Oinas, and M. I. Mishchenko (2004), Calculation of radiative fluxes from the surface to top of atmosphere based on ISCCP and other global data sets: Refinements of the radiative transfer model and the input data, *J. Geophys. Res.*, *109*, D19105, doi:10.1029/2003JD004457.

Zhou, L., et al. (2003), Comparison of seasonal and spatial variations of albedos from Moderate-Resolution Imaging Spectroradiometer (MODIS) and Common Land Model, *J. Geophys. Res.*, *108*(D15), 4488, doi:10.1029/2002JD003326.

Zhu, X. F., S. L. Liang, Y. Z. Pan, and X. T. Zhang (2011), Agricultural irrigation impacts on land surface characteristics detected from satellite data products in Jilin Province, China, *IEEE J. Sel. Top. Appl. Earth Obs. Remote Sens.*, *4*(3), 721–729, doi:10.1109/jstars.2011.2106152.